Int. J. Electrochem. Sci., 11 **(2016)** 10847 – 10862, doi: 10.20964/2016.12.96

International Journal of
ELECTROCHEMICAL
SCIENCE
www.electrochemsci.org

Polyol mediated synthesis and electrochemical performance of nanostructured $LiMn_2O_4$ cathodes

Shuo Yang[1], *Melanie Homberger*[1,2], *Michael Noyong*[1,2], *Ulrich Simon*[1,2,*]

[1] Institute of Inorganic Chemistry, RWTH Aachen University, Landoltweg 1, 52074 Aachen, Germany
[2] JARA-FIT, 52056 Aachen, Germany.
[*]E-mail: ulrich.simon@ac.rwth-aachen.de

Received: 26 August 2016 / *Accepted:* 15 October 2016 / *Published:* 10 November 2016

Nanoparticulate single phase $LiMn_2O_4$ spinel was prepared via polyol method and applied as a cathode in a lithium ion battery. The effects of calcination temperature (250 °C – 800 °C) as well as of post-synthetic treatment by ball milling on the physiochemical and electrochemical properties of $LiMn_2O_4$ were studied by means of powder XRD, SEM, cyclic voltammetry and charge/discharge cycling. With increasing calcination temperature, the electrochemical activity and discharge capacity increased. The measurements revealed that the electrochemical performance of $LiMn_2O_4$ can be further improved by ball milling before calcination. Furthermore, the ball milling process allowed reducing the calcination temperature needed to obtain electrochemically active material.

Keywords: Lithium ion battery, $LiMn_2O_4$ spinel, nanoparticles, calcination, ball milling

1. INTRODUCTION

In the past decades, $LiMn_2O_4$ spinel has been extensively studied as one of the promising cathode candidates for large scale lithium ion batteries owing to the inexpensive and environmentally benign Mn as the redox active metal, high rate capability and good safety [1–4]. In the spinel structure, the oxygen form a cubic-close-packed lattice, whereas the lithium and manganese ions occupy the tetrahedral (8a) and octahedral (16d) sites, respectively, as illustrated in Figure 1. This crystal structure offers a three-dimensional network of diffusion paths for the rapid diffusion of Li^+ ions during insertion and extraction. $LiMn_2O_4$ exhibits a potential of 4 V versus Li/Li^+ when cycled over the composition range of $Li_xMn_2O_4$ ($0 \leq x \leq 1$), delivering a theoretical capacity of 148 mAh/g.

However, a challenge accompanied with this material is the capacity fading during cycling, especially at elevated temperature. Xia et al. summarized the major detrimental effects that are responsible for the capacity fading [5]. Among these effects, the most striking ones are: (i) dissolution of Mn^{2+} into the electrolyte due to disproportionation of Mn^{3+} into Mn^{4+} and Mn^{2+} [6] and (ii) the onset of Jahn-Teller distortion when cycled below 3 V [7]. As a possibility to overcome these challenges and to further improve the electrochemical performance of $LiMn_2O_4$, the following strategies have been followed so far: partial substitution of Mn by bi- or trivalent cations such as Co [8], Ni [9], or Al [10], fluoride doping [11] and surface modification, e.g. by coating with oxides [12]. A further approach, which is discussed in the research community, is the use of nanostructured materials with high control over size and morphology [13–16]. Nanostructured materials offer the advantages of short diffusion path lengths for lithium-ion transport as well as better accommodation of strain during lithium insertion/extraction. Moreover, the rate performance can be improved owning to the large surface area of nanostructured materials [17,18]. Nonetheless, by reducing the particle sizes of $LiMn_2O_4$, the dissolution of Mn may be exacerbated due to increased contact surface area between $LiMn_2O_4$ and the electrolyte [19].

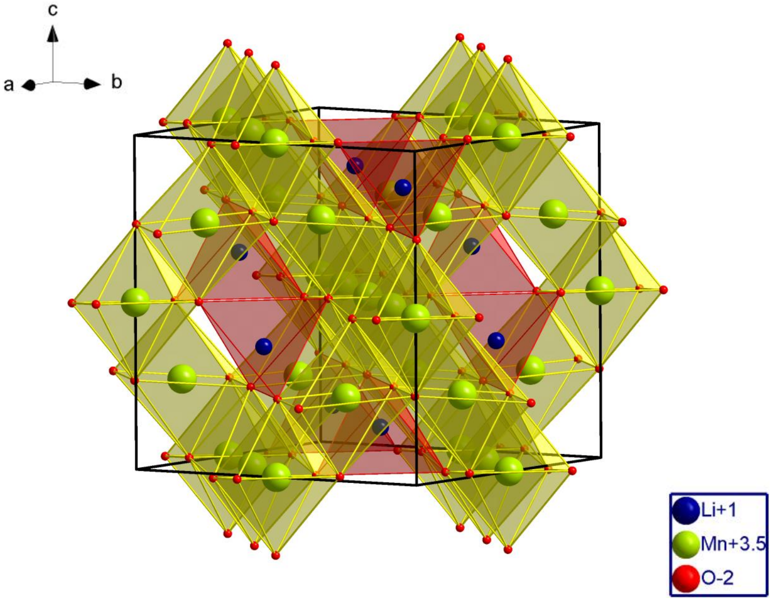

Figure 1. Crystal structure of $LiMn_2O_4$ (yellow: MnO_6 octahedra; red: LiO_4 tetrahedra).

Conventionally $LiMn_2O_4$ is synthesized via a solid state method, which includes long and repeated heat treatment processes at high temperature as well as extended grinding [7]. It is, therefore, difficult to control the particle size and surface morphology of the final product.

Previously, the preparation of nanostructured binary metal oxides via the polyol method was frequently reported [20,21]. In those works the authors demonstrated the highly effective role of polyol in controlling the particle size and morphology. The polyol method has been also proven to be successful in preparing cathode materials for lithium ion batteries, such as $LiFePO_4$ [22], $LiMnO_2$ [23] and $LiMnPO_4$ [24]. The preparation of $LiMn_2O_4$ via the polyol method was first reported by Gerand et al. [25]. They applied electrolytic manganese dioxide (EMD) and lithium hydroxide in ethylene glycol (EG). According to their results, a calcination step at higher than 200 °C is necessary in order to initiate the formation of the spinel phase. Calcination at 800 °C resulted in electrochemically active material. However, they did not perform systematic electrochemical investigations on the effect of calcination temperatures. In another publication from this group, they reported a similar polyol mediated synthesis approach, where they reported a platelet morphology of particles calcined at 800 °C [26].

Based on these investigations we prepared $LiMn_2O_4$ adopting the polyol-approach introduced by Gerand et al. and analyzed the effect of different calcination temperatures between 250 °C and 800 °C on the physiochemical and electrochemical properties of $LiMn_2O_4$. In addition, we introduced ball milling as an additional treatment step of the as-synthesized material in order to investigate its effect on the material properties. Our investigations include powder XRD, SEM, cyclic voltammetry, and charge/discharge cycling. We found that the electrochemical activity and discharge capacity increased with increasing calcination temperature. Additionally, the electrochemical performance could be further improved by introducing a ball milling process before calcination. The additional ball milling process before calcination allowed reducing the calcination temperature needed to obtain highly electrochemical material.

2. EXPERIMENTAL

2.1. Polyol synthesis of $LiMn_2O_4$

$LiMn_2O_4$ particles were synthesized *via* the polyol method followed by calcination in air, adopting the polyol-approach introduced by Gerand et al.. 1.56 g LiOH (Merck, >98%) and 2.83 g electrolytic manganese oxide (EMD, grade HMR-AF, Tosoh, 92.5%) were dissolved and dispersed, respectively, in 50 mL ethylene glycol (EG, Fluka, >99.5%). The suspension was heated up to 160 °C at a heating rate of 1 $°C·min^{-1}$ under reflux and vigorous stirring. The temperature was maintained at 160 °C for 17 h and cooled down to room temperature at a cooling rate of 1 $°C·min^{-1}$. A thermal controller (model 2416, Eurotherm) was used to monitor and control the reaction temperature. Afterwards, the precipitates were recovered by vacuum filtration, washed twice with acetone (Fisher, p.A.) and dried under vacuum at room temperature for 3 h. The as-synthesized powders were calcined at 250, 500, 600, 700 or 800 °C in air in two steps (Table 1). First, the samples were heated up at a slow heating rate of 10 $°C·min^{-1}$ to 250 °C and kept at 250 °C for 10 h. Afterwards sample LMO-250 (Table 1) was directly cooled down to room temperature at a cooling rate of 1 $°C·min^{-1}$. The samples LMO-500, LMO-600, LMO-700 and LMO-800 (see Table 1) were heated up to the respective temperature at a heating rate of 1 $°C·min^{-1}$. After reaching the final calcination temperature each sample was kept at this temperature for 24 h and then cooled down to room temperature applying the same condition as for LMO-250.

Additionally, the as-synthesized powders were subjected to a ball milling process before calcination. The ball milling process was performed in a ZrO_2 grinding bowl equipped with ZrO_2 grinding balls at a rotation speed of 200 rpm for 60 min, using a planetary ball mill (Pulverisette 7 premium line, Fritsch GmbH). After the ball milling process, the ground powders were calcined at 600 °C (LMO-BM-600), 700°C (LMO-BM-700) and 800°C (LMO-BM-800), respectively, according to the above described procedure.

Table 1. Sample name and treatment.

Sample Name	Calcination Temperature (°C)	Ball Milling Before Calcination
as-synthesized	No	No
LMO-250	250	No
LMO-500	250 and 500	No
LMO-600	250 and 600	No
LMO-BM-600		Yes
LMO-700	250 and 700	No
LMO-BM-700		Yes
LMO-800	250 and 800	No
LMO-BM-800		Yes

2.2. Characterization

2.2.1. Physiochemical characterization

Powder X-ray diffraction (XRD) measurements were conducted at room temperature using a Stoe STADI P diffractometer (Stoe & Cie GmbH) operating in transmission mode with Cu $K_{\alpha 1}$ radiation (λ=1.54059 Å). The acquired powder XRD data were processed with the softwares WinXPOW.

The powder morphology was analyzed using a high resolution field emission scanning electron microscope (FE-SEM) Leo Supra 35 VP (Zeiss).

2.2.2. Cathode sheet preparation

The cathode sheets were prepared by coating an active material containing slurry on aluminum foil. The slurry was prepared by mixing and ultrasonically dispersing 81.6 wt% of active material, 10.4 wt% of super C 65 carbon (IMERYS Graphite & Carbon), which serves as conductive agent, and 8.0 wt% of polyvinylidene fluoride (PVDF, Aldrich) as binder in N-Methyl-2-pyrrolidone (NMP, Aldrich). It was coated on aluminum foil (Western Plastics) using a Mayer rod with a wet thickness of 50 µm. Afterwards the coated foil was dried at 100 °C, punched out with a diameter of 16 mm and transported into an argon-filled glove box.

2.2.3. Electrochemical characterization

For the electrochemical tests, ECC-Std test cells or ECC-Air test cells with blocked gas inlet and outlet (EL-Cell) were assembled in an argon-filled glove box with LMO cathodes, lithium metal (ø=18 mm, Alfa Aesar) as anode, 100 µL 1 M $LiPF_6$ (Aldrich) in 1:1 (w:w) mixture of ethylene carbonate (EC, Aldrich) diethyl carbonate (DEC, Aldrich) as electrolyte and a glass fiber separator (ø=18 mm, t=260 µm, Whatman). The configurations of the test cells are shown in Figure S1 in the Supporting Information.

The electrochemical tests were performed on a Basytec LAB battery tester (Basytec GmbH). The electrochemical properties of the calcined samples were characterized by cyclic voltammetry (CV). The cell potential ranged from 3.5 V to 4.5 V at a scan rate of 0.02 $mV \cdot s^{-1}$.

The specific discharge capacities of the investigated samples were determined by charging and discharging between 3.5 V and 4.5 V with a constant current of C/20 followed by a 30-minute constant voltage charge/discharge for 10 cycles. The C-rate was calculated with the theoretical capacity of $LiMn_2O_4$, i.e.148 mAh/g.

3. RESULTS AND DISCUSSION

3.1. Effect of different calcination temperatures

The crystal structures of the samples calcined at different temperatures (250°C, 500°C, 600°C, 700°C, 800°C) were analyzed by powder XRD. According to the powder XRD patterns shown in Figure 2, all samples exhibited single cubic spinel phase with the space group Fd-3m, which is in agreement with literature [25,26]. Although the spinel phase appeared already in the sample LMO-250, its diffraction peaks are broad and have low intensities, which indicates poor crystallinity and/or a small crystallite size. With increasing calcination temperature, the diffraction peaks became sharper and the intensities rose, which indicates improved crystallinity. According to these measurements, high crystallinity was obtained at calcination temperatures of 700 and 800 °C.

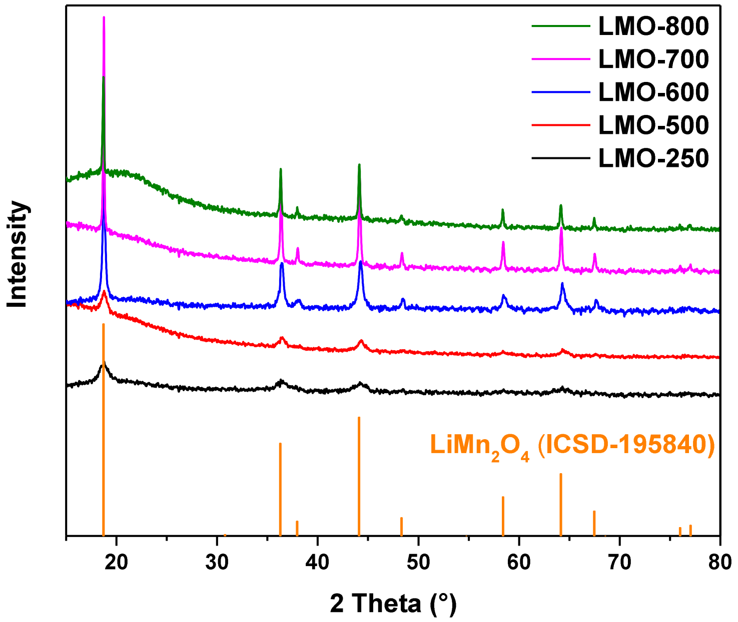

Figure 2. XRD patterns of as-synthesized LMO powders calcined at different temperatures, in agreement with literature data [25–27].

The materials calcined at different temperatures were also analyzed by SEM measurements in order to investigate the particle size and morphology. The obtained images are shown in

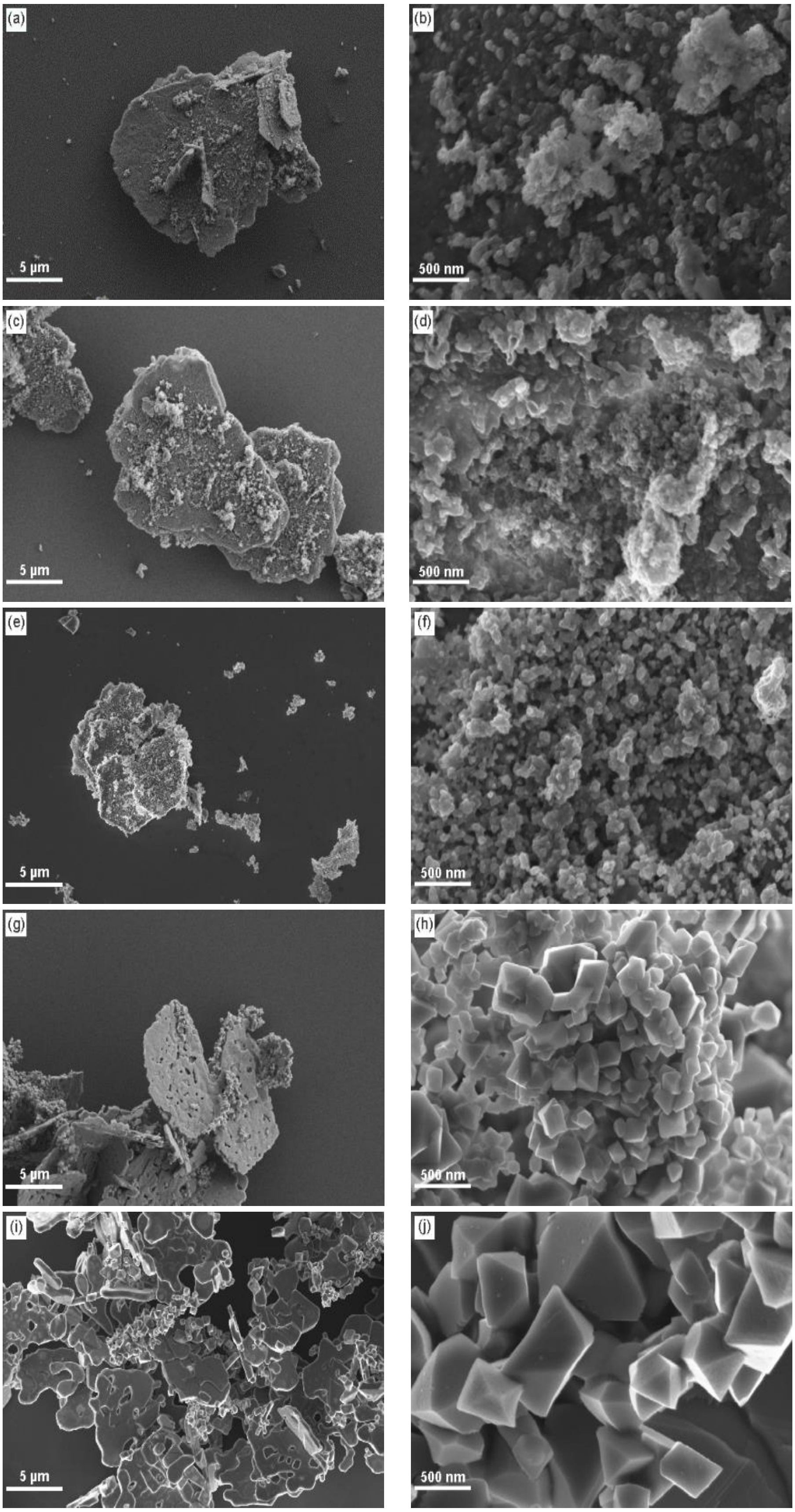

Figure 3. SEM micrographs of samples LMO-250 (a, b), LMO-500 (c, d), LMO-600 (e, f), LMO-700 (g, h), and LMO-800 (i, j).

Similar to the investigations of Larcher et al. [26], we observed in all samples platelets with a size of about 10 µm besides almost spherical (at low calcination temperatures) or octahedral (at high calcination temperatures) nanoparticles . The platelet morphology, which was also observed in the as-synthesized powders before calcination (see Figure S2(a) in the Supporting Information) retained after calcination. In contrast to that, the nanoparticles, which can also be observed in the as-synthesized material (see Figure S2(b) in the Supporting Information), grew in size and adopted gradually octahedral shape with increasing calcination temperature. The particle size rose from about 30 nm to about 500 nm, when the calcination temperature was raised from 250 °C to 800 °C. In the sample LMO-800 several particles with a particle size of 1-3 µm were also visible, shown in

The powder XRD results discussed above confirmed that secondary phases were not detectable in all samples. Therefore, it is assumed that both platelets and nanoparticles share the same crystal structure.

The electrochemical properties of the calcined samples were evaluated by cyclic voltammetry. The cyclic voltammograms are shown in Figure 4. Reversible electrochemical processes at around 4 V were observed in all samples. At low calcination temperatures (250 °C and 500 °C), the recorded current was low and only one broad redox peak was observed. This indicates that the materials exhibited low crystallinity, which is in accordance with the powder XRD measurements, and low electrochemical activity. With increasing calcination temperatures up to 700 °C, the current response enlarged and two well-split redox peaks were recorded, indicating improved electrochemical activity. These two redox peaks, situated at 4.02/3.99 V and 4.14/4.12 V, correspond to the two-step reversible (de)intercalation of lithium between $LiMn_2O_4$ and γ-MnO_2 [7], which is characteristic of materials with high degree of crystallinity. However, no obvious further improvement was gained by raising the calcination temperature from 700 °C to 800 °C. This result is in accordance with the powder XRD measurements. It has to be noted that the sample LMO-250 showed faintly also two redox couples, the reason behind remains still unclear. We assume that the crystalline domains in the sample LMO-250 might have been recrystallized during further calcinations

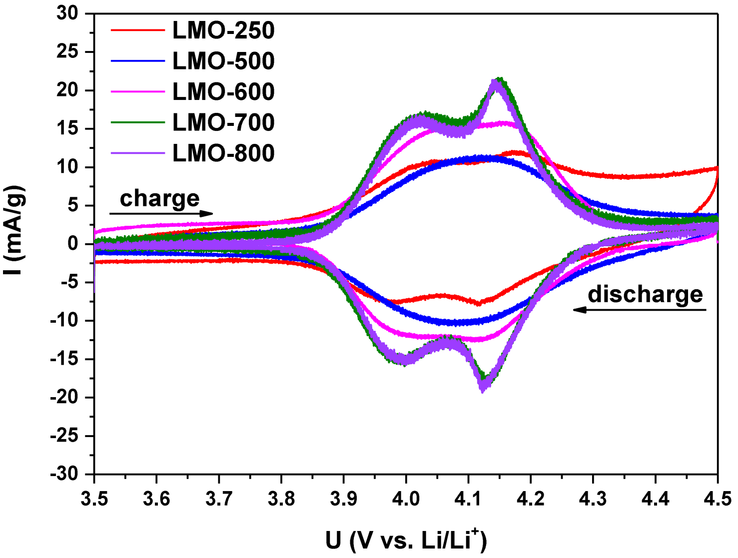

Figure 4. Cyclic voltammograms of LMO calcined at different temperatures (250, 500, 600, 700 and 800 °C).

According to these results, a calcination temperature of at least 600 °C seems to be necessary to obtain materials with sufficient electrochemical activity. Concerning the determination of specific discharge capacity, we therefore, focused on the samples calcined at 600 °C, 700 °C and 800 °C.

Figure 5 shows the determined specific discharge capacities of samples LMO-600, LMO-700 and LMO-800 and the values are summarized in Table 2. At the 1st cycle, the samples LMO-600, LMO-700 and LMO-800 delivered specific discharge capacities of 55.5 mAh/g, 73.8 mAh/g and 75.3 mAh/g, respectively. It is obvious that the specific discharge capacity of the investigated samples increased significantly, when the calcination temperature increased from 600 °C to 700 °C. A slight increase of the specific discharge capacity was observed, when the calcination temperature was raised from 700 °C to 800 °C. This improvement in discharge capacity can be attributed to the enhanced crystallinity with increasing calcination temperature. All of the investigated samples (LMO-600, LMO-700 and LMO-800) exhibited excellent stability with capacity retention of 96.2 %, 96.6 % and 100 % after 10 cycles, respectively. The measured capacities of the calcined samples are comparable to the values reported in literature of micro-scaled $LiMn_2O_4$ [28,29].

Table 2. Specific Discharge Capacities of LMO-600, LMO-700 and LMO-800.

Sample	Specific Discharge Capacity (mAh/g)		Capacity Retention after 10 Cycles (%)
	1st cycle	10th cycle	
LMO-600	55.5	53.4	96.2
LMO-700	73.8	71.3	96.6
LMO-800	75.3	76.7	100[1]

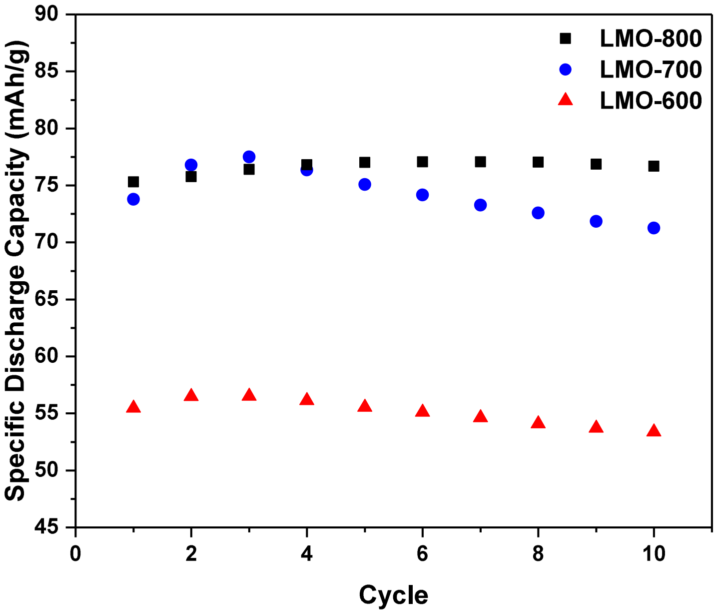

Figure 5. Specific discharge capacity determination with C/20 of samples LMO-700 and LMO-800.

---

[1] Capacity retention = 100 %, when the capacity at 10th cycle is equal or larger than the one at 1st cycle.

However, they are still relatively low compared with the theoretical discharge capacity of $LiMn_2O_4$. Except for the large particle size, the platelet morphology in the samples may also be a limiting factor for the capacities. Due to the low electric conductivity of $LiMn_2O_4$, the intercalation/deintercalation of Li^+ ions can only occur at the junctions, where active material, conductive carbon and electrolyte are in contact. Therefore, the large platelets in the samples may also limit their capacities, especially when the conductive carbon is distributed inhomogeneously on the particle surface. Our approach to eliminate the platelets is to introduce an additional ball milling process before calcination. The influence of ball milling on the crystal structure, particle morphology and electrochemical properties are discussed in the next section.

3.2. Effect of ball milling

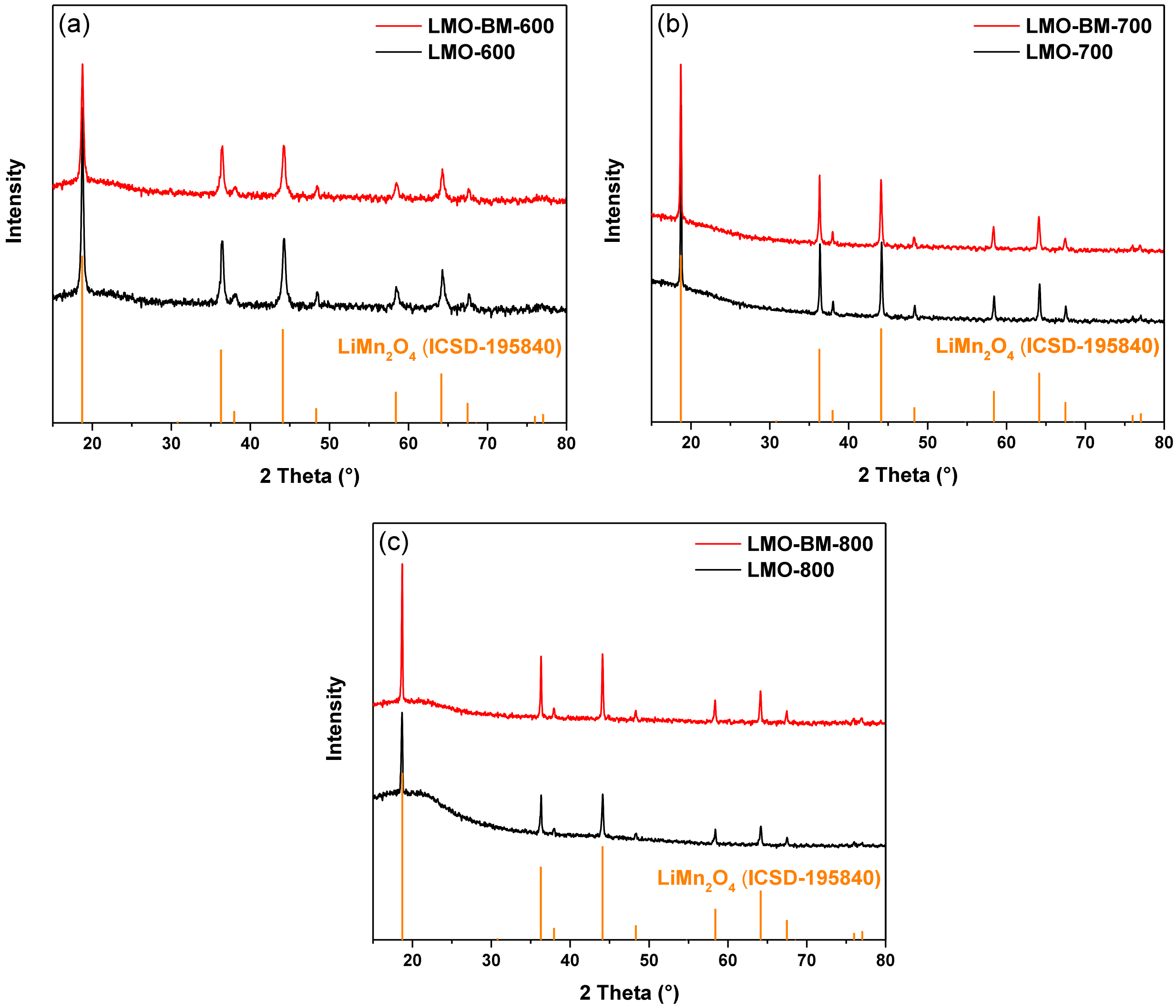

Figure 6. XRD patterns of samples LMO-BM-600 (a), LMO-BM-700 (b) and LMO-BM-800 (c).

The comparison of the XRD pattern of samples LMO-BM-600, LMO-BM-700 and LMO-BM-800, treated by ball milling before calcination, with the samples LMO-600, LMO-700 and LMO-800 are shown in Figure 6(a), (b) and (c), respectively. It is obvious that no structural change was introduced by the ball milling process in all samples. Pure $LiMn_2O_4$ spinel phase with high crystallinity was obtained.

Nonetheless, the morphology of the samples was influenced by the ball milling process, as shown in Figure 7. The platelets, which were retained after calcination in the samples without ball milling, were successfully eliminated in the ball-milled samples, whereas the nanoparticles remain unaffected compared to those in the samples LMO-600, LMO-700 and LMO-800. The average sizes of the nanoparticles in the samples LMO-BM-600, LMO-BM-700 and LMO-BM-800 are about 50 nm, 100 nm and 500 nm respectively. Octahedra with larger particle sizes (500 nm – 1 µm in sample LMO-BM-700, 1-2 µm in sample LMO-BM-800) can be observed in both LMO-BM-700 and LMO-BM-800 samples.

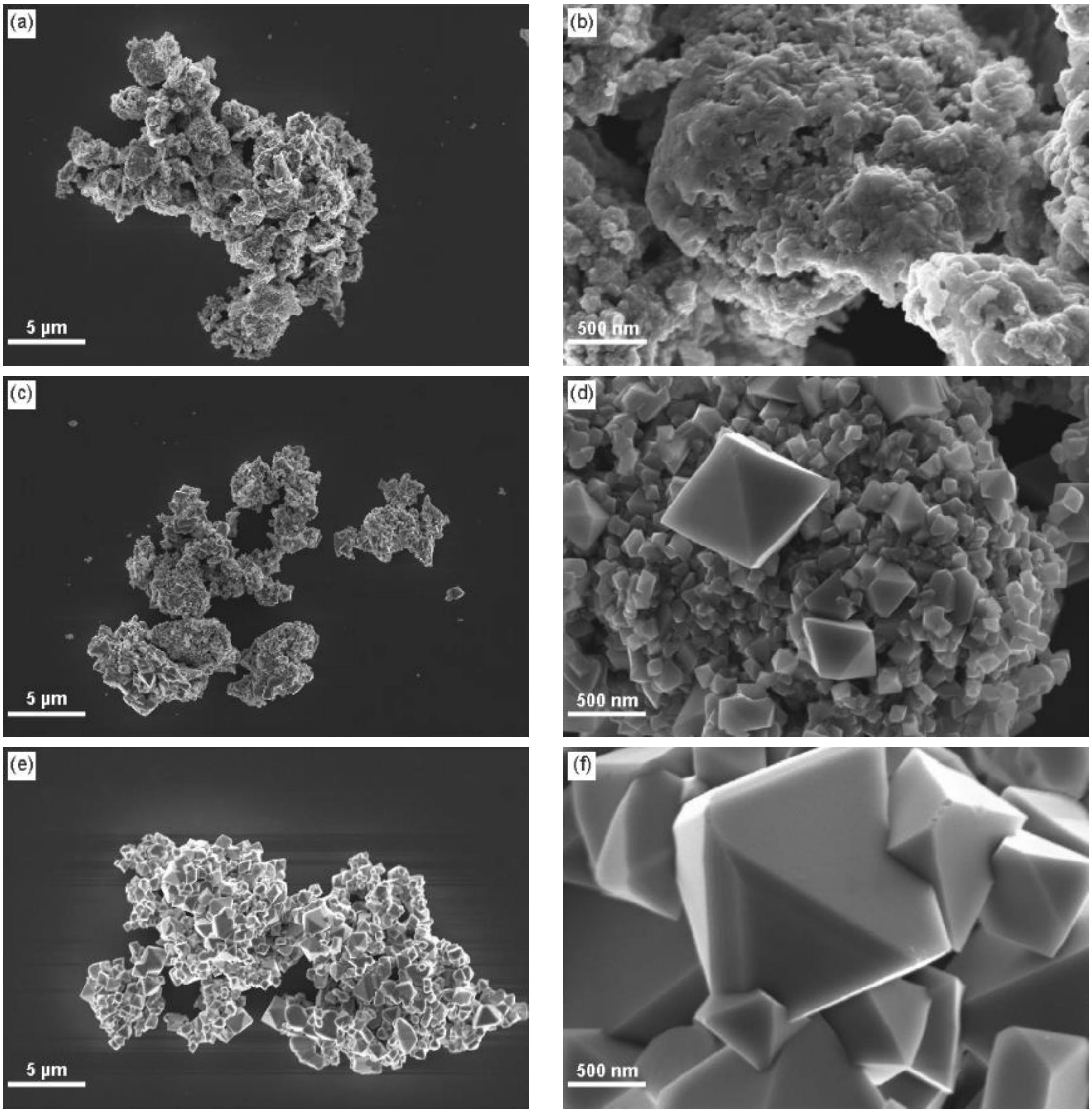

Figure 7. SEM micorgraphs of samples LMO-BM-600 (a, b), LMO-BM-700 (c, d) and LMO-BM-800 (e, f).

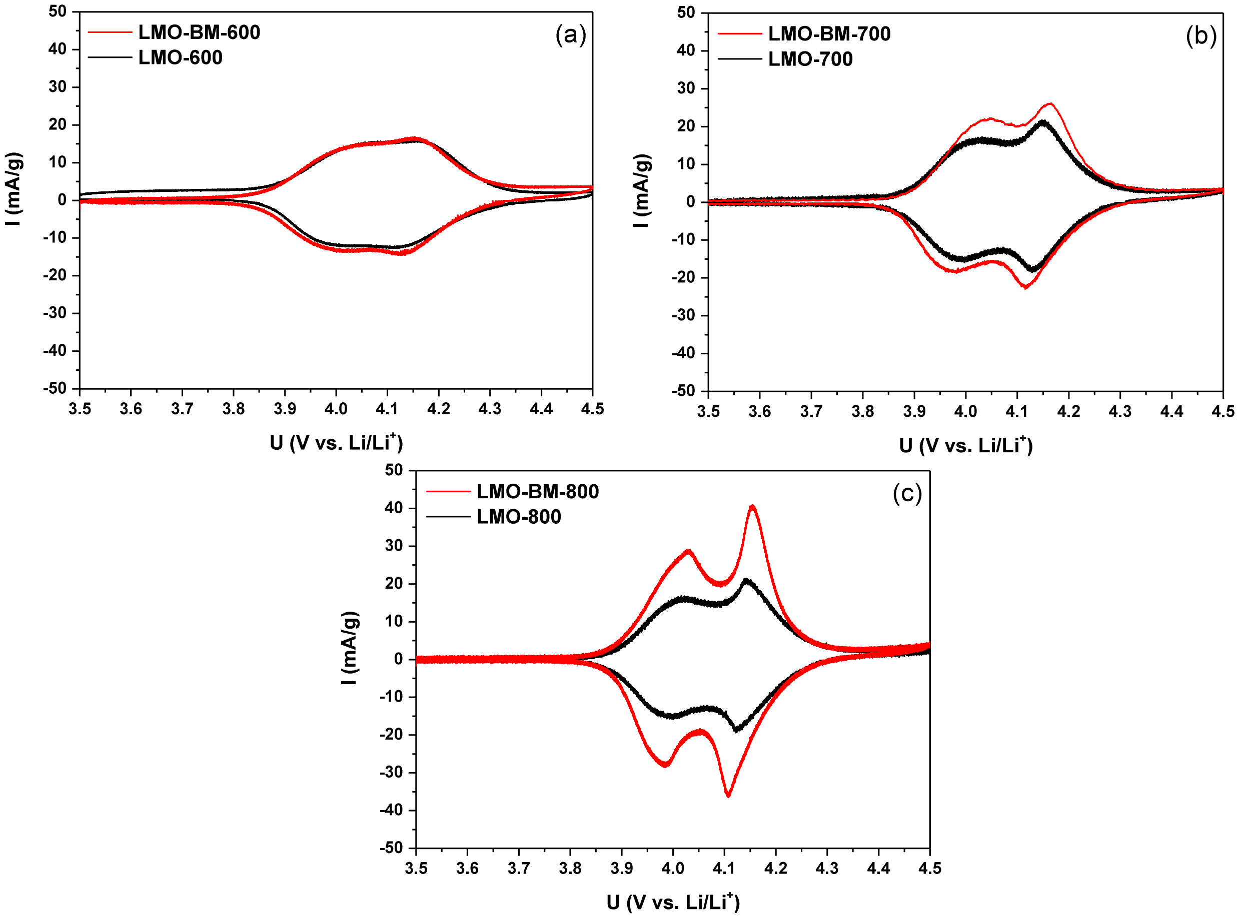

Figure 8. Cyclic voltammograms of ball milled samples (in red) LMO-BM-600 (a), LMO-BM-700 (b) and LMO-BM-800 (c) and their comparison with non-milled samples (in black).

The cyclic voltammograms of samples treated by ball milling (LMO-BM-600, LMO-BM-700 and LMO-BM-800; in red) are plotted and compared with the non-milled samples (in black) in Figure 8. The recorded current response of sample LMO-BM-600 was approximately the same as that of sample LMO-600. This indicates that the electrochemical activity of LMO-BM-600 was comparable to that of LMO-600, i.e. the electrochemical activity of the 600 °C-calcined sample was unaffected by the ball milling process. When the calcination temperature was raised to 700 °C, an increase of the current response can be observed in the sample LMO-BM-700 compared to LMO-700. This suggests an improvement of the electrochemical activity by ball milling. The two redox peaks observed in sample LMO-700 were present in sample LMO-BM-700, too, and have similar shape. This result is consistent with the powder XRD patterns. When the calcination temperature reached 800 °C, the increase of the current response was enlarged, indicating enhanced improvement of the electrochemical activity. The two redox peaks of LMO-BM-800 are more clearly defined than in the case of the sample LMO-800. Previous cyclic voltammetry studies related to the influence of LMO film and particle morphology on the electrochemical performance attributed more clearly resolved redox peaks at low scan rates (0.1 $mV \cdot s^{-1}$, compared to 0.02 $mV \cdot s^{-1}$ in our work) to an improved crystallinity [30-32]. According to these findings our result may indicate that the crystallinity of LMO-

BM-800 is superior than that of LMO-800 though the powder XRD studies do not reflect any structural differences.

Table 3. Specific Discharge Capacities of LMO Samples with Additional Ball Milling Process.

Sample	Specific Discharge Capacity (mAh/g)		Capacity Retention after 10 Cycles (%)
	1st cycle	10th cycle	
LMO-BM-600	61.2	62.5	100[2]
LMO-BM-700	82.0	80.4	98.1
LMO-BM-800	90.6	92.3	100

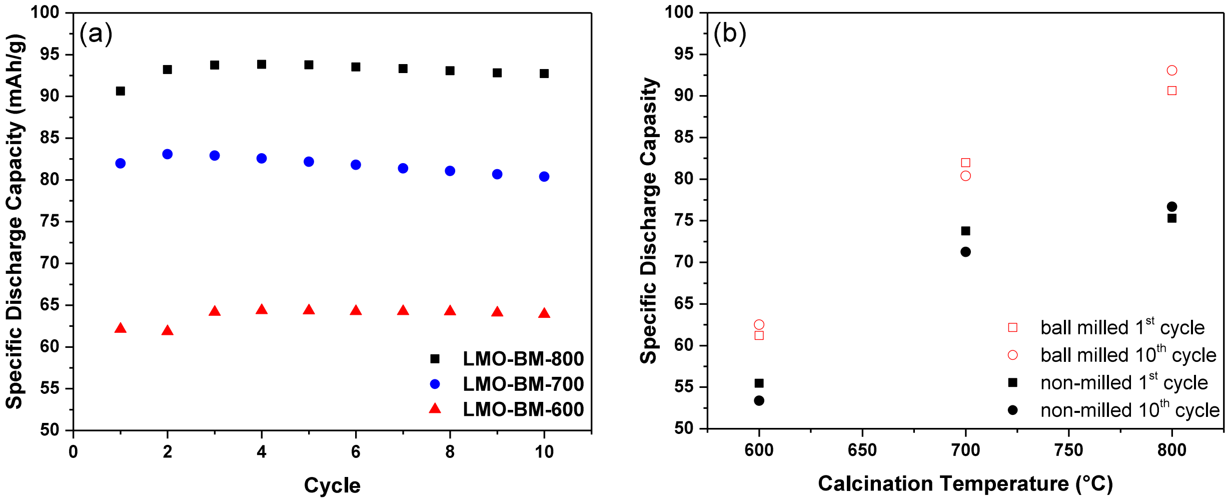

Figure 9. Specific discharge capacity determination with C/20 of ball milled samples (a), and comparison of the effect of ball milling of non-milled and ball milled samples (b).

Figure 9 (a) shows the determined specific discharge capacities of samples LMO-BM-600, LMO-BM-700 and LMO-BM-800. All of the ball milled samples exhibited excellent stability with capacity retention of 100 %, 98.1 % and 100 % after 10 cycles, respectively. The specific discharge capacities of the ball milled samples were compared with the ones of the non-milled samples (see Figure S3 in the Supporting Information). The specific discharge capacities of these samples at the 1st and the 10th cycles, which are also summarized in Table 3, are compared with the non-milled samples in Figure 9(b). At the 1st cycle, the samples LMO-BM-600, LMO-BM-700 and LMO-BM-800 delivered specific discharge capacities of 61.2 mAh/g, 82.0 mAh/g and 90.6 mAh/g, respectively, which were by 10.3 %, 11.1 % and 20.4 % higher than the specific discharge capacities of sample LMO-600, LMO-700 and LMO-800, respectively. We are absolutely aware about the fact that the obtained specific discharge capacities are lower than values reported in previous studies related to LMO [16,30,33]. However, a comparable discharge capacity (85 mAh/g) was already reported by another group [28] for LMO particles in the similar size range and the focus within our study was on determining trends resulting from the different treatment of the prepared materials with less attention to the absolute values of the capacity. Considering the observed trends our results clearly indicate that the specific discharge capacities were indeed improved by the ball milling process. We suppose that by

---

[2] Capacity retention = 100 %, when the capacity at 10th cycle is equal or larger than the one at 1st cycle.

eliminating the platelet morphology by ball milling, larger portions of the active material contributed to the discharge capacity. According to our results, this improvement is more significant with increasing calcination temperature, which may be attributed to the improved crystallinity, indicated by CV. Our results can be related to previously investigations concerning the influence of the particle morphology, i.e. the surface orientation, of $LiNi_{0.5}Mn_{1.5}O_4$ (LMNO) on the electrochemical performance [43]. Thereby LMNOplatelets in the size range of 2 µm (100 nm thickness) yielded lower discharge capacities in a wide range of charging rates (C/22 – 3C) than octahedral particles in the same size range, which was assigned to different kinetics and reactivity of the different crystal plane orientation. It is worth noting that the specific discharge capacity of sample LMO-BM-700 is even higher than that of sample LMO-800. This suggests that by introducing an additional ball milling process before calcination, the calcination temperature needed to obtain highly electrochemical material can be reduced.

4. CONCLUSION

In this work we presented the synthesis of $LiMn_2O_4$ via polyol method and investigated the effect of different calcination temperature as well as an additional ball milling step before calcination on the physiochemical and electrochemical properties. According to powder XRD patterns, although the spinel phase existed already at lower temperatures, a calcination temperature of at least 600 °C is necessary to ensure sufficient crystallinity. SEM micrographs revealed two different morphologies present in all samples: platelets with a size of about 10 µm as well as nanoparticles. The nanoparticles adopt with increasing calcination temperature gradually an octahedral shape. CV revealed that the electrochemical activity of the investigated samples was improved with increasing calcination temperature. The specific discharge capacity increased from 55.5 mAh/g (LMO-600) to 75.3 mAh/g (LMO-800) with increasing calcination temperature.

In order to eliminate the observed platelets and to investigate, if the electrochemical performance can be improved, an additional ball milling step was applied before calcination. Powder XRD showed no influence of the ball milling process on the crystallinity of the samples. According to the SEM micrographs, the platelet morphology was successfully eliminated and furthermore the nanoparticulate octahedra remained unaffected. CV measurements revealed that the electrochemical activity of the samples was indeed improved. The specific discharge capacity was improved by ball milling. This improvement became more significant with increasing calcination temperature.

Well-crystallized $LiMn_2O_4$ with a specific discharge capacity of 90.6 mAh/g was prepared by calcination at 800 °C with a ball milling process before calcination, whereas the specific discharge capacity of the ball milled sample calcined at 700 °C is even higher than that of the non-milled sample calcined at 800 °C. Accordingly the additional ball milling process before calcination allowed reducing the calcination temperature needed to obtain highly electrochemical material, which will be beneficial for an optimized utilization of resources.

ACKNOWLEDGEMENT

Financial support by the DFG Research Training Group 1856 "MobilEM" is gratefully acknowledged. We thank Brigitte Hermanns for assistance with the synthesis. We are also immensely grateful to the Institute for Power Electronics and Electrical Drives at RWTH Aachen University for part of the electrochemical measurements.

SUPPORTING INFORMATION

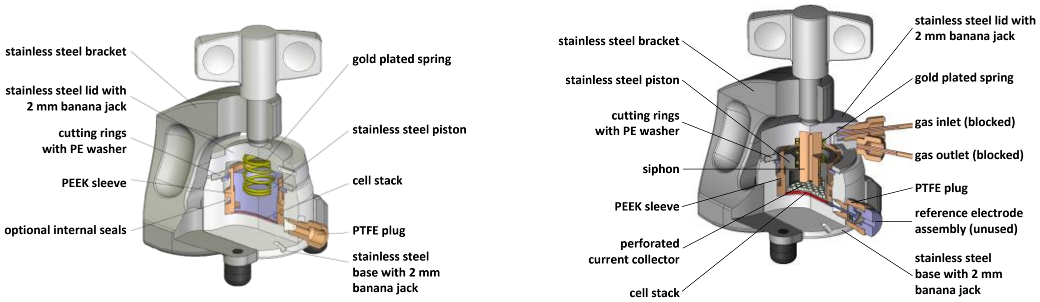

(a) (b)

Figure S1. Configurations of the test cells(a) ECC-Std and (b) ECC-Air.

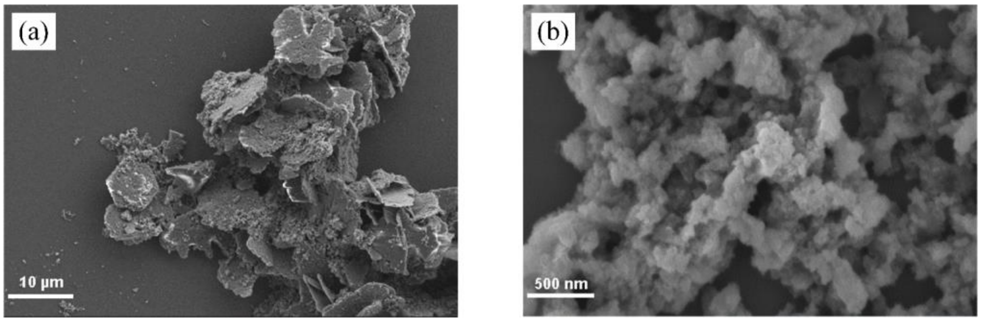

Figure S2. SEM micrographs of as-synthesized material. (a) platelets with a size of about 10 µm and agglomerates of nanoparticles were visible in the as-synthesized material; (b) nanoparticles with a size of about 10 nm.

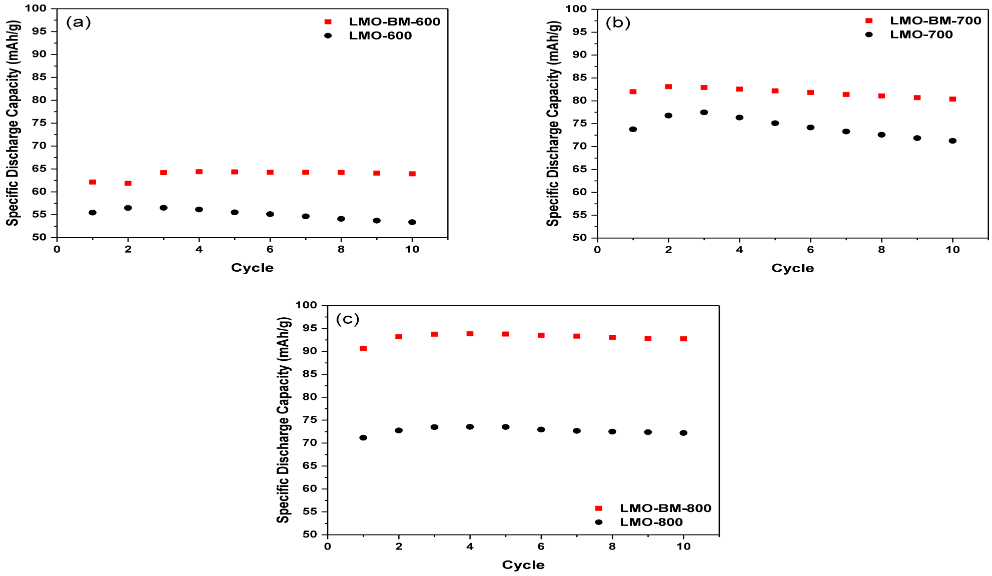

Figure S3. Comparison of the specific discharge capacity determination with C/20 of ball milled samples with non-milled samples calcined at (a) 600 °C, (b) 700 °C and (c) 800 °C.

References

1. M. M. Thackeray, W. David, P. G. Bruce and J. B. Goodenough, *Materials Research Bulletin,* 18 (1983) 461.
2. M. M. Thackeray, *Progress in Solid State Chemistry,* 25 (1997) 1.
3. A. Manthiram, *J. Phys. Chem. Lett.,* 2 (2011) 176.
4. S. Dou, *Ionics,* 21 (2015) 3001.
5. H. Xia, Z. Luo and J. Xie, *Progress in Natural Science: Materials International,* 22 (2012) 572.
6. D. H. Jang, *J. Electrochem. Soc.,* 143 (1996) 2204.
7. M. M. Thackeray, P. J. Johnson, L. A. de Picciotto, P. G. Bruce and J. B. Goodenough, *Materials Research Bulletin,* 19 (1984) 179.
8. S. Mandal, R. M. Rojas, J. M. Amarilla, P. Calle, N. V. Kosova, V. F. Anufrienko and J. M. Rojo, *Chem. Mater.,* 14 (2002) 1598.
9. H. M. Wu, J. P. Tu, X. T. Chen, Y. Li, X. B. Zhao and G. S. Cao, *J. Solid State Electrochem.,* 11 (2006) 173.
10. Y. L. Ding, J. Xie, G. S. Cao, T. J. Zhu, H. M. Yu and X. B. Zhao, *J. Phys. Chem. C,* 115 (2011) 9821.
11. Q. Luo and A. Manthiram, *J. Electrochem. Soc.,* 156 (2009) A84.
12. T.-F. Yi, Y.-R. Zhu, X.-D. Zhu, J. Shu, C.-B. Yue and A.-N. Zhou, *Ionics,* 15 (2009) 779.
13. D. K. Kim, P. Muralidharan, H.-W. Lee, R. Ruffo, Y. Yang, C. K. Chan, H. Peng, R. A. Huggins and Y. Cui, *Nano Letters,* 8 (2008) 3948.
14. H.-W. Lee, P. Muralidharan, R. Ruffo, C. M. Mari, Y. Cui and D. K. Kim, *Nano Letters,* 10 (2010) 3852.
15. J.-Y. Luo, H.-M. Xiong and Y.-Y. Xia, *J. Phys. Chem. C,* 112 (2008) 12051.
16. M.-K. Song, S. Park, F. M. Alamgir, J. Cho, M. Liu, *Mater. Sci. Eng.* R 72 (2011) 203-252
17. A. Manthiram, A. Vadivel Murugan, A. Sarkar and T. Muraliganth, *Energy Environ. Sci.,* 1 (2008) 621.
18. U. K. Sen, S. Sarkar, P. S. Veluri, S. Singh and S. Mitra, *Nanoscience & Nanotechnology-Asia,* 3 (2013) 21.
19. K. Matsuda and I. Taniguchi, *J. of Power Sources*, 132 (2004) 156.
20. H. Dong, Y.-C. Chen and C. Feldmann, *Green Chem.,* 17 (2015) 4107.
21. M. Siemons, A. Leifert and U. Simon, *Adv. Funct. Mater.,* 17 (2007) 2189.
22. R. Muruganantham, R. Subadevi and M. Sivakumar, *AMR*, 584 (2012) 341.
23. D. Larcher, B. Gérand and J.-M. Tarascon, *International Journal of Inorganic Materials,* 2 (2000) 389.
24. T. R. Kim, D. H. Kim, H. W. Ryu, J. H. Moon, J. H. Lee, S. Boo and J. Kim, *J. . Phys. Chem. Sol.,* 68 (2007) 1203.
25. B. Gerand, D. Larcher and J.-M. Tarascon, Process for synthesizing $Li_xMn_yO_4$ intercalation compounds, U.S. Patent 5747193 (1998).
26. D. Larcher, B. Gérand and J.-M. Tarascon, *J. . Solid State Electrochem.*, 2 (1998) 137.
27. A. K. Jahja, T. Nugraha, A. Fajar and E. Kartini, *Indonesian Journal of Materials Science,* (2009) 123.
28. M. A. Kiani, M. F. Mousavi and M. S. Rahmanifar, *Int. J. Electrochem. Sci*, 6 (2011) 2581.
29. Y. Sun, C. Xu, B. Li, J. Xu, Y. He, H. Du and F. Kang, *Int. J. Electrochem. Sci,* 9 (2014) 6387.
30. A. Rougier, K. A. Striebel, S. J. Wen, E. J. Cairns, *J. Electrochem. Soc.*, 145 (1998) 2975-2980, 1998.

31. D. Singh, R. Houriet, R. Giovannini, H. Hofmann, V. Craciun, R.K. Singh, *J. Power Sources* 97-98 (2001) 26–831.
32. Proceedings of the 10th International Meeting on Lithium Batteries, July 2001; D. Singh, R. Houriet, R. Vacassy, H. Hofmann, V. Cracium, R. K. Singh in Subbarao Surampudi, *Electrochemical Society Meeting - Lithium Batteries: Proceedings of the International Symposium*, ISBN 1566772486, 9781566772488, pp 371-378, The Electrochemical Society, New Jersey, USA 2000.
33. Q. Li, C. Peng, J. Huang, W Xu, F Yang, Hongli Bai, C. Su, J. Guo, *Int. J. Electrochem. Sci.* 10 (2015) 7513 – 7520.
34. B. Hai, A. K. Shukla, H. Duncan, G. Chen, *J. Mater. Chem. A* 1 (2013), 759–769.